Materials Science & Engineering A 621 (2015) 265–271

Contents lists available at ScienceDirect

Materials Science & Engineering A

journal homepage: www.elsevier.com/locate/msea

Microstructural evolution of a delta containing nickel-base superalloy during heat treatment and isothermal forging

P.M. Mignanelli [a], N.G. Jones [a,*], K.M. Perkins [b], M.C. Hardy [c], H.J. Stone [a]

[a] Department of Materials Science and Metallurgy, University of Cambridge, Cambridge CB3 0FS, UK
[b] Swansea University, Institute of Structural Materials, College of Engineering, Singleton Park, Swansea SA2 8PP, UK
[c] Rolls-Royce plc, PO BOX 31, Derby DE24 8BJ, UK

ARTICLE INFO

Article history:
Received 19 September 2014
Received in revised form
24 October 2014
Accepted 27 October 2014
Available online 6 November 2014

Keywords:
Nickel-base superalloys
Thermomechanical processing
Electron microscopy
Microstructure

ABSTRACT

The next generation of aerospace gas turbine engines need to operate at higher temperatures and stresses to improve their efficiency and reduce emissions. These operating conditions are beyond the capability of existing nickel-base superalloys, requiring the development of new high temperature materials. Controlling the microstructures of these new materials is key to obtaining the required properties and, therefore, it is critical to understand how these alloys respond to processing and heat treatment. Here, the microstructural evolution of V207M, a new δ containing, nickel-base superalloy, has been investigated following heat treatment and forging. The solvus temperatures of the γ′ and δ phases, determined by differential scanning calorimetry and microscopy, were found to be ~985 and ~1060 °C respectively. Isothermal forging of the alloy was conducted at 1000, 1050 and 1100 °C, corresponding to different volume fractions of retained δ. Considerable softening was observed prior to steady state flow when forging at 1000 °C, whilst only steady state flow occurred at 1050 and 1100 °C. The steady state flow process was believed to be dominated by dynamic recovery in the γ phase, with an activation energy of 407 kJmol^{-1}. Samples that exhibited flow softening also showed a significant change in the orientation of the δ precipitates, preferentially aligning normal to the forging axis, and this reorientation was thought to be the cause of the observed flow softening.

1. Introduction

Stringent emissions targets for the aerospace industry are driving the need for new, more efficient gas turbine engines, operating at higher temperatures and increased rotational speeds [1,2]. The strenuous conditions experienced by components in the turbine section have pushed current nickel-base superalloys to their serviceable limits and has led to significant research into alternative material solutions [3]. Despite showing promise, the mechanical and environmental properties of many of the alternatives do not yet offer sufficient benefits for their adoption in critical components [4–6]. Therefore, the need to increase the temperature capablity of nickel-base superalloys remains of critical importance.

The polycrystalline nickel-base superalloys used for disc applications typically consist of a nickel A1 (Strukturbericht notation) matrix, γ, reinforced by coherent $L1_2$ superlattice precipitates, γ′, which convey the high temperature properties for which these alloys are renowned. Higher temperature capability can be obtained by increasing the volume fraction of γ′, which is usually achieved by adding greater concentrations of the γ′ forming elements Al, Ti and Ta [7,8]. Nb also stabilises the γ′ phase and has recently been shown to be effective in controlling the γ′ size distribution [9]. However, the behaviour of the matrix is also critical, and so modern alloys contain Cr for environmental resistance as well as Mo, Co and W to provide solid solution strengthening.

Powder-processing is preferred over a cast and wrought approach when producing such highly alloyed materials as it enables greater control over the microstructure and elemental segregation [10,11]. After compaction through hot isostatic pressing (HIP), thermo-mechanical processing (TMP) is often used to break up the prior particle boundaries that persist after the HIP stage [12]. High forging temperatures can result in hot shortness and cracking, whilst the forging stresses at low temperatures become unacceptably high, requiring specialised dies, and can lead to inhomogeneous deformation of the alloy as well as fracture of the forging [13,14]. Therefore, it is essential to develop an understanding of an alloy's deformation behaviour and microstructural response during TMP operations.

During the forging of superalloys, the mechanisms of recovery and recrystallisation compete and dominance depends upon the deformation conditions; temperature, strain and strain rate. At high strain rates and lower temperatures flow behaviour tends to

* Corresponding author. Tel.: +44 1223 334367.
E-mail address: ngj22@cam.ac.uk (N.G. Jones).

http://dx.doi.org/10.1016/j.msea.2014.10.071

be dominated by dynamic recrystallisation of the γ phase, giving rise to flow softening at low strains [15,16]. In contrast, deformation at higher temperatures and lower strain rates exhibits steady state flow, dominated by dynamic recovery [16].

Alloys with high concentrations of Nb may also contain precipitates of δ – Ni_3Nb ($D0_a$ structure), which typically form as high aspect ratio plates, in addition to the γ and γ′ phases. Previous studies investigating the forging of δ containing alloys have observed that this phase has a considerable effect upon the deformation behaviour, causing pronounced flow softening at low strains [17,18]. However, the underlying mechanism for this softening has yet to be conclusively established.

Flow curves obtained from δ processed Inconel 718 exhibited flow softening and the acicular δ precipitates were seen to fragment and spheroidise [19,20]. However, γ grain refinement was also observed and, due to the similarity of the flow curves to those of conventionally processed Inconel 718, it was thought that dynamic recrystallisation, rather than δ evolution, dominated the observed behaviour [19]. In contrast, a recent study on the deformation behaviour of a γ–γ′–δ eutectic alloy found that the δ precipitates did not fragment during forging, but rotated to become aligned with the direction of material flow [21]. Significant softening was observed in the corresponding flow curves at all but the highest temperatures, yet the dominating deformation mechanism was not established, instead being referred to as dislocation based plasticity. However, it is clear that the determination of the dominant deformation mechanism was complicated by the significant fraction of γ′ present in the material, as γ′ precipitates have been observed to inhibit recrystallisation in Udimet 720 when forged >30 °C below its γ′ solvus temperature [22].

To determine suitable industrial processing parameters and clarify the role of δ precipitates on the flow behaviour, the reponse of V207M, a newly developed γ′ strengthened and δ containing nickel-base superalloy [23] has been characterised following isothermal forging. Systematic heat treatments were used to determine the microstructural evolution of the γ′ and δ phases and provide evidence of the high temperature microstructures prior to deformation. Isothermal forging was subsequently completed across a range of strain rates and temperatures to investigate the influence of microstructural condition on flow behaviour. Critically, due to the significant temperature difference between the γ′ and δ solvi of this alloy, it was possible to assess the influence of the δ precipitates on the flow behaviour of the material independent of the γ′ phase. As a result, the observed flow softening could be directly related to the rotation of the δ precipitates, whilst steady state flow was dominated by dynamic recovery of the γ phase.

2. Experimental procedure

Argon gas atomised powder was produced by ATI Powder Metals and supplied as a compact following hot isostatic pressing. The target composition of the alloy and the supplier's measured values are shown in Table 1. The measured composition of the alloy was in good agreement with the target values, with all elements within 0.25 at% of the target concentration.

Differential scanning calorimetry (DSC) was completed using a Netzsch 404 high temperature calorimeter, at heating and cooling rates of 10 °C per minute under an argon atmosphere. Analysis of the heating curve, combined with complimentary microscopy, enabled the identification of the γ′ and δ solvus temperatures.

Heat treatments of 35 min, typical of current industrial forging practices, were conducted on samples encapsulated in glass ampoules backfilled with argon to minimise oxidation at temperatures between 900 and 1150 °C, followed by water quenching. Metallographic preparation was completed to a 0.25 μm finish and the samples were electrolytically etched in phosphoric acid at 3–5 V or by immersion in Kalling's reagent (where stated). Light micrographs were acquired using a Leica optical microscope and secondary electron images (SEI) obtained from a JEOL 6340 FEGSEM. Identification of the δ precipitates from the SEI was completed manually before quantitative analysis of the microstructures using the ImageJ software package, as shown in Fig. 1. Electron Backscatter Diffraction (EBSD) measurements were made using an FEI Nova NanoSEM 450 fitted with a Bruker e^-Flash^{1000} detector.

Isothermal forging of V207M was completed using cylinders of 6.3 mm diameter and 8.3 mm length taken from the as-HIP compact. Specimens were inserted into the pre-heated furnace and given a 35 min soak, to ensure thermal equilibrium. Compression testing was completed using a servo-hydraulic ESH 016606 rig, with two N-type thermocouples attached to either side of the lower platen. The testing matrix consisted of three temperatures: 1000, 1050 and 1100 °C and three strain rates: 0.01, 0.003 and 0.001 s^{-1}. Testing was completed to a true strain of 0.7 whereupon the sample was water quenched. Samples were subsequently sectioned and imaged with the vertical axis parallel to the forging direction.

3. Results and discussion

3.1. Microstructural response of V207M to thermal treatment

The microstructure of the as-HIP V207M compact is shown in Fig. 2. The relatively coarse prior particle boundary network, resulting from the powder processing route, can be seen in Fig. 2a. As mentioned in the introduction, such features are potentially detrimental to the mechanical properties of the alloy and need to be broken up by subsequent TMP operations. The alloy contained three main microstructural constituents, γ, γ′ and δ, which can be seen more clearly in Fig. 2b and c. The δ precipitates existed as high aspect ratio lathes within the γ grains, with typical dimensions of ~1–5 μm in length and less than 0.5 μm in width. The γ′ existed in a spherical morphology, with a diameter of ~100 nm. Quantitative image analysis was used to obtain the volume fraction of the two precipitate phases, which were determined to be 29% δ and 18% γ′.

A DSC thermogram, obtained during heating of the as-HIP material, is given in Fig. 3. Several endothermic events were observed, corresponding to phase transformations within the material. The γ′ and δ phases are both known to re-solution into the γ phase above their respective solvus temperatures and evidence of such solid state phase transformations were observed by the occurrence of two peaks below 1100 °C. These features are

Table 1
Target and measured compositions of V207M in at% (target composition from [23]).

at%	Ni	Cr	Co	Fe	Mo	W	Al	Nb	Ta	Ti	C	B	Zr
Target	bal.	19.0	4.0	9.0	0.35	0.9	5.5	3.5	0.7	1.0	0.15	0.15	0.035
Measured	bal.	19.25	4.0	8.91	0.33	0.89	5.34	3.47	0.71	1.0	0.08	0.17	0.036

shown more clearly in the inset, where the peak temperatures have been marked, ~970 °C and ~1067 °C. It should be noted that these temperatures correspond to the maximum rate of precipitate dissolution rather than the true solvus temperatures for each phase [24], but nevertheless they provide a useful guide. However, unambiguously attributing each event to the appropriate phase is not possible without additional information, such as in-situ diffraction data or supplementary metallographic imaging.

Identification of the phase transformations associated with the two transitions of interest observed in the DSC thermogram was achieved by characterisation of the microstructure following heat treatment between 900 and 1150 °C for 35 min, Fig. 4. Phase volume fractions were quantified using image analysis and are presented in Fig. 5. The volume fraction of secondary γ′ was only considered, since the formation of tertiary γ′ was believed to be a consequence of the quenching process, rather than being present at the heat treatment temperature. The volume fractions of both the γ′ and δ phases present at 900 °C, Fig. 4a, are similar to those of the as-HIP material, Fig. 2, suggesting that little microstructural change occurred over this timescale at lower temperatures. At temperatures between 900 and 1000 °C the volume fraction of the γ′ phase was observed to decrease, Fig. 4a–e, whilst, concurrently, the volume fraction of δ was observed to increase slightly up to 950 °C, Fig. 5. This is likely to be a consequence of an elevated level of Nb in the matrix, liberated by the dissolution of the γ′ phase, which enabled increased δ precipitation. Above 975 °C the δ phase volume fraction decreased, persisting in the microstructure up to 1050 °C, Fig. 4d–g. However, there was no evidence of the δ phase after heat treatment at 1100 °C, Fig. 4h. Linear extrapolation of the phase volume fractions produced solvus temperatures of ~985 °C for the γ′ phase and ~1060 °C for the δ phase. These results correlate well with the transitions observed in the DSC data.

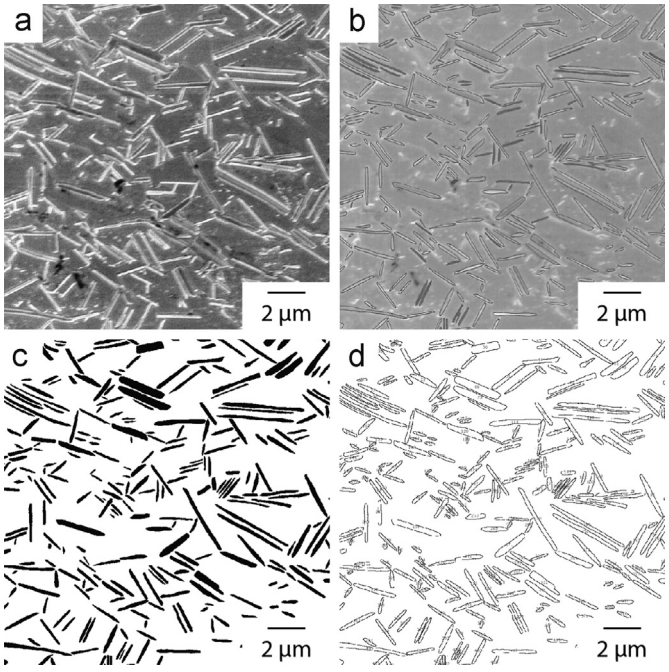

Fig. 1. Steps of the quantitative image analysis methodology used to characterise secondary phases, showing (a) the original micrograph, (b) the identification of δ precipitates, (c) thresholding to a binary image and (d) the analysed δ precipitates from ImageJ.

In the as-HIP condition, forging above the γ′ solvus is potentially desirable as it reduces the load experienced by the tooling. In addition, greater damage tolerance and dwell fatigue resistance has reduced the requirement for very fine grain sizes, which were previously obtained through sub-solvus processing using the γ′ to restrict grain growth [25]. Therefore, from the results of the heat treatment studies, three temperatures were identified for forging trials. These were; 1000 °C, just above the γ′ solvus but with a significant volume fraction of δ; 1050 °C, just below the δ solvus such that the majority of material was in the γ phase; and 1100 °C, in the γ phase field.

3.2. Isothermal forging of V207M

Forging of V207M at each of the selected temperatures was conducted at three strain rates: 0.01, 0.003 and 0.001 s^{-1}. The associated flow curves are shown in Fig. 6 from which the influence of temperature, strain rate, and microstructure on the deformation behaviour of the alloy can be inferred. Due to the limited amount of material available for this study, repeat testing of every experimental condition was not possible. However, where duplicate measurements were made, the flow curves obtained exhibited minimal deviation to those shown in Fig. 6. Therefore, it is believed that the behaviours shown in this figure are representative of the material's response.

In all cases, the material deformed elastically up to yield at low strains. When forged at 1050 and 1100 °C (Fig. 6b and c) the alloy showed limited work hardening beyond the yield point before a steady state flow condition was achieved. The observed flow stress of the alloy decreased when forged at higher temperatures or slower strain rates. This behaviour is common during forging, as the change in temperature and strain rate influences the dislocation density in the material and the subsequent mechanisms of recovery, recrystallisation and work hardening in the alloy [26–28]. In contrast to higher temperature forging, deformation

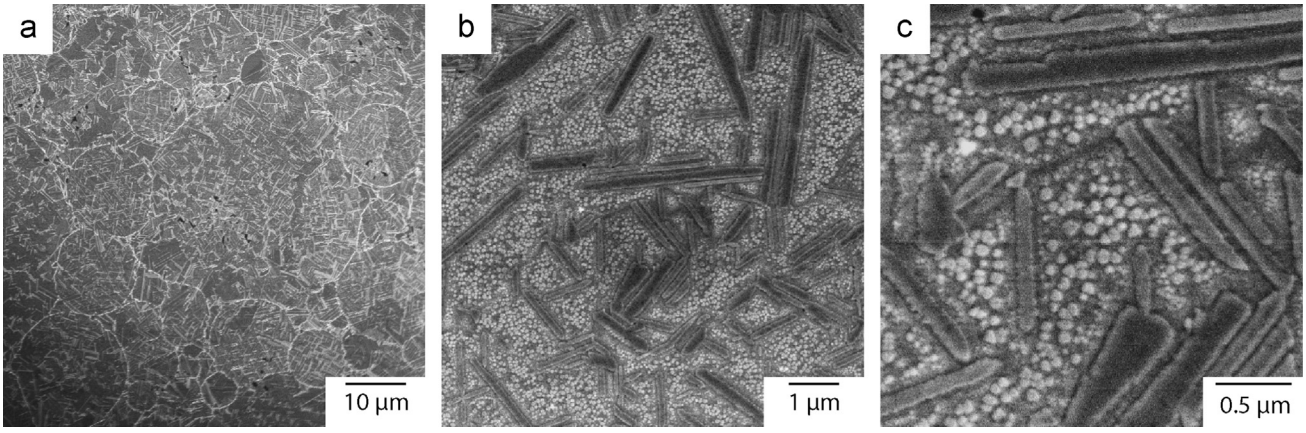

Fig. 2. SEI images of the microstructure of the V207M as-HIP compact following etching with phosphoric acid.

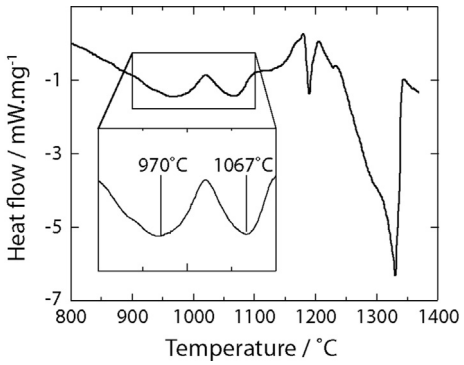

Fig. 3. DSC thermogram from as-HIP condition V207M during heating.

at 1000 °C exhibited work hardening to a peak stress at a true strain of ~0.05, followed by considerable flow softening before reaching steady state flow at ~0.5 true strain.

The peak and flow stresses measured across all forging conditions are presented in Table 2. In addition, the ratio of peak stress to flow stress (σ_{PFR}) for each of the forging conditions was calculated according to Eq. (1). For a given forging temperature, the value of σ_{PFR} was found to be independent of strain rate and, therefore, a mean value ($\bar{\sigma}_{PFR}$) is presented in Table 2, along with the associated standard deviation. This ratio illustrates the change between the initial and steady state flow behaviours at 1000 °C, where $\bar{\sigma}_{PFR} > 1.45$, and at temperatures above 1050 °C, where $\bar{\sigma}_{PFR} < 1.1$. Notably, if all of the steady state flow stresses are considered as a function of temperature and strain rate they are

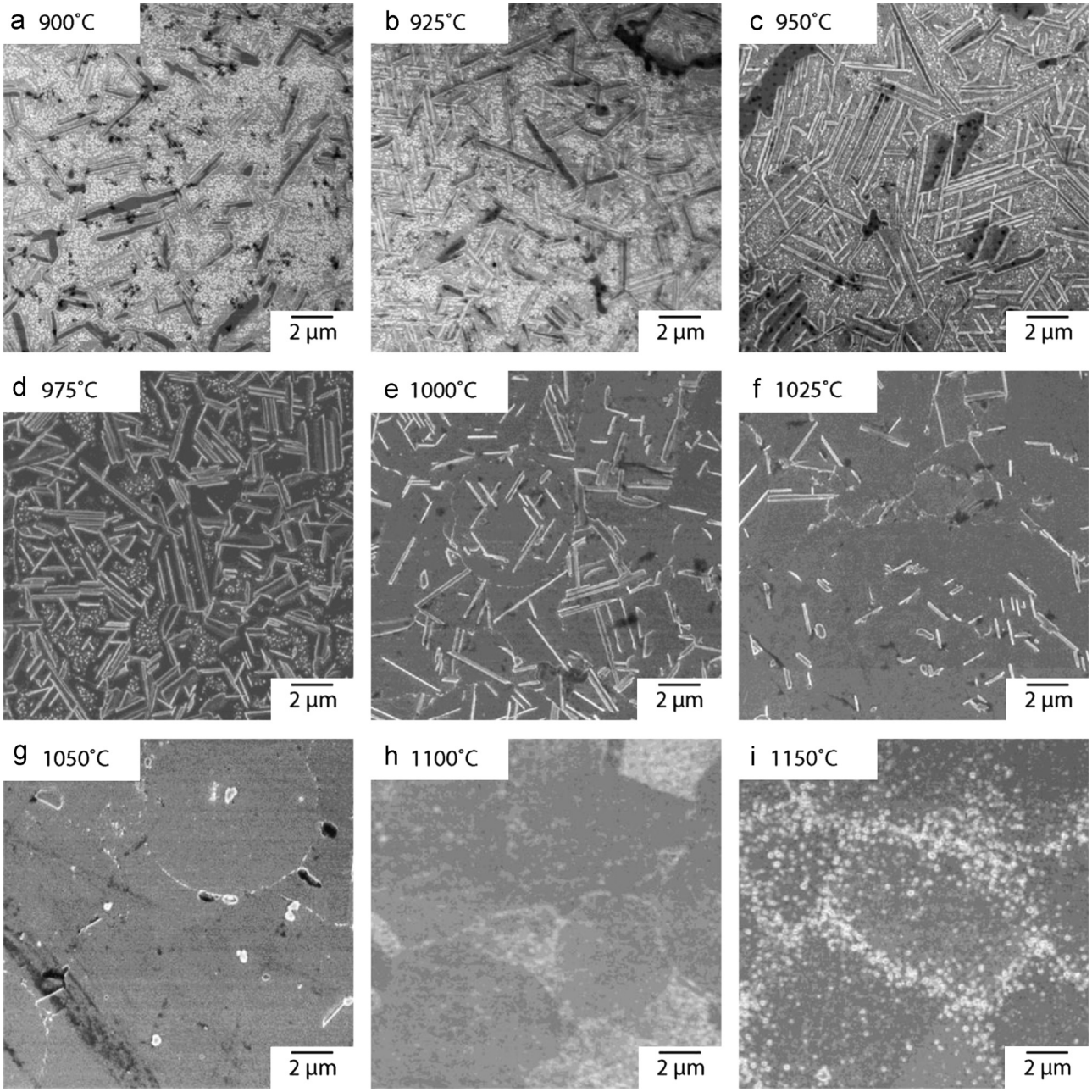

Fig. 4. SEI showing alloy V207M following heat treatment between 900 and 1150 °C for 35 min, etched with phosphoric acid.

well described by a power law relationship.

$$\sigma_{PFR} = \frac{\text{peak stress}}{\text{flow stress}} \quad (1)$$

Using this principle, the activation energy for steady state flow was calculated using a multiple linear regression, as outlined by Sellars and McTegart [29], Eq. 2, where $\dot{\varepsilon}$ is the strain rate, A, α and n' are material constants, σ is the stress, Q is the activation energy for hot deformation, R is the gas constant and T is the absolute temperature.

$$\dot{\varepsilon} = A(\sinh \alpha\sigma)^{n'} \exp(-Q/RT) \quad (2)$$

The activation energy for steady state flow was calculated to be 407 kJmol^{-1}, which is in excellent agreement with the work of Detrois et al. [19], who obtained a value of 400 kJmol^{-1} for a ternary eutectic γ–γ′–δ alloy. It is also in good agreement with the reported values of many other nickel-base superalloys [30–32]. The similarity of these activation energies suggests that the same mechanism is dominating the steady state flow behaviour across a wide range of compositions. If this is the case, then this mechanism must relate to the γ phase, as this was the only phase present at 1100 °C.

Flow softening in nickel-based superalloys is often attributed to recrystallisation [33–36]. However, no evidence of significant grain refinement was observed in V207M. Optical microscopy of the as-HIP condition and material forged at 1100 °C with a strain rate of 0.01 s^{-1} is shown in Fig. 7. The grain structure of the as-HIP material, Fig. 7a, showed little variation to that of the dead zone in the forged sample, where the strain is minimal, Fig. 7b. The similar grain sizes indicated that static recrystallisation had not occurred at 1100 °C. The grain structure at the centre of the forged sample, where strain is at its maximum, is shown in Fig. 7c. As expected, the grains had become elongated perpendicular to the forging direction, but there was no evidence of grain refinement, which would be indicative of dynamic recrystallisation. The grain size of the sample forged at 1000 °C and a strain rate of 0.01 s^{-1} could not be satisfactorily resolved by optical microscopy due to the presence of the δ phase. Therefore, the grain structure at the centre of this sample was evaluated from a band contrast image acquired from EBSD mapping, Fig. 7d. Although these grains do not appear to be elongated, the average size is comparable to that of Fig. 7c, especially when discounting twin boundaries and the dark features in the underlying image that correspond to the δ phase. These results suggest that extensive dynamic recrystallisation had not occurred and that, therefore, the observed flow softening in V207M is dependent upon an alternative mechanism.

The absence of recrystallised grains in the sample forged in the single phase condition at 1100 °C, suggested that the dominant mechanism of steady state flow must be dynamic recovery of the γ phase. This process involves dislocation climb, which is analogous to vacancy diffusion. The activation energy for self diffusion in pure nickel is 287 kJmol^{-1}, well below the experimentally realised value. The large difference in these energies may be due to the significant solute content of the γ phase, ~43 at% in V207M. This would also be true for similar commercial alloys where the nickel content is commonly less than 60 at%, and may explain why the activation energies reported for these alloys are all in the region of 400 kJmol^{-1} [30–32].

Flow softening has also been related to microstructural evolution during forging, for example the fragmentation of acicular precipitates, such as δ in Inconel 718 [19] and α in metastable beta titanium alloys [37–39]. Representative microstructures from the centre of the forged samples, typical of all the considered strain rates, are shown in Fig. 8. The volume fraction of δ precipitates was similar to that of the prior static heat treatment samples, see Fig. 4, indicating that applied strain did not significantly influence the dissolution kinetics of this phase. A detailed comparison of the pre- and post-forged microstructures obtained at 1000 °C, Fig. 4e

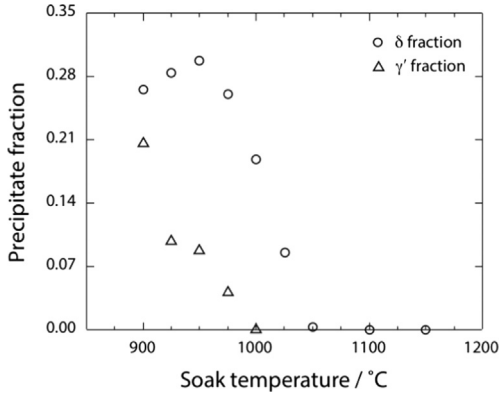

Fig. 5. Measured volume fractions of γ′ and δ phases in V207M following heat treatment between 900 and 1150 °C for 35 min.

Table 2
Summary of the peak and flow stresses of V207M from Fig. 6.

Temperature/ °C	Strain rate/s^{-1}						Ratio of peak to flow stress (σ_{PFR})
	0.01		0.003		0.001		
	Peak stress	Flow stress	Peak stress	Flow stress	Peak stress	Flow stress	
1000	198	137	155	106	112	72	1.488 (±0.059)
1050	118	113	93	84	63	59	1.073 (±0.032)
1100	91	83	68	64	45	43	1.068 (±0.025)

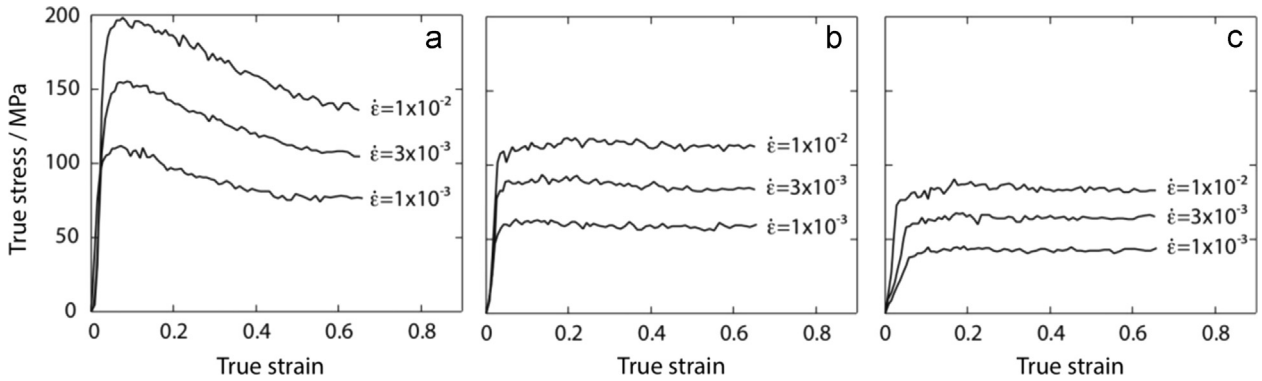

Fig. 6. Flow curves of V207M during forging at (a) 1000 °C (b) 1050 °C and (c) 1100 °C.

and Fig. 8a respectively, revealed no significant alteration in the precipitate morphology, thereby eliminating δ fragmentation as a softening mechanism. However, following forging, the δ precipitates had a preferential orientation, with their major axis aligned parallel to the direction of material flow (horizontal to the page). This observation suggested that the flow softening that occurred during forging might be related to the re-orientation of the hard δ precipitates.

Quantitative image analysis was used to characterise the angle of the δ precipitates with respect to the forging axis. Analysis was performed on the central regions of all the samples forged at 1000 °C and from a representative area of the as-HIP compact. The normalised frequency of the δ orientations relative to the forging axis is presented in Fig. 9. The δ phase is known to have a well-documented orientation relationship with the γ grains [40], but in a polycrystalline material it can be thought to have a random macroscopic orientation due to the indiscriminate arrangement of the γ grains in the initial powder processed material. In the as-HIP compact, Fig. 9a, there was no correlation between the δ precipitate orientation and the sample axes, demonstrating that sufficient parent γ grains had been sampled. In contrast, the corresponding histograms for the samples forged at 1000 °C, Fig. 9b–d, showed a considerable anisotropy in the distribution of δ orientation, and a preferential alignment perpendicular to the forging axis. The alignment of the δ precipitates was most pronounced at the fastest strain rate, Fig. 9d, yet the difference in σ_{PFR} for the three different strain rates was minimal. A similar rotation of the δ precipitates was reported by Detrois et al. [19] when forging a γ–γ′–δ eutectic alloy. In their work, strain rate was also reported to influence the δ orientation distribution, in a similar manner to that shown in Fig. 9. This suggests that strain rate may have an effect on the final orientation distribution, however, its influence on the flow softening behaviour is currently inconclusive.

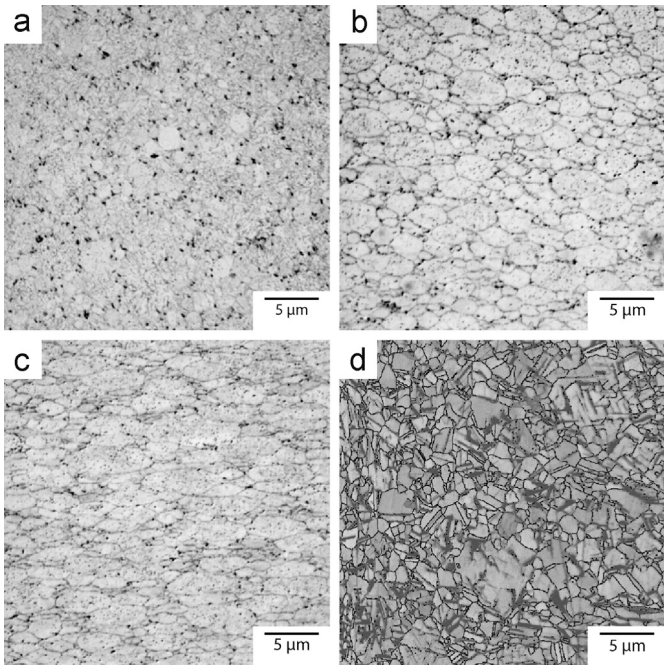

Fig. 7. Optical micrographs of V207M comparing the microstructures in (a) the as-HIP compact, and following forging at 1100 °C and 0.01 s^{-1} in (b) the dead zone and (c) the sample centre, all etched with Kalling's reagent and (d) EBSD band contrast map of the grain boundaries from the centre of the sample forged at 1000 °C and 0.01 s^{-1}.

4. Conclusions

The microstructure of V207M, a new δ precipitate containing nickel-base superalloy, has been characterised following heat treatment and isothermal forging from an as-HIP state. The solvus temperatures of the γ′ and δ phases were determined to be ~985 and ~1060 °C respectively when evaluated by both differential thermal analysis and metallographic techniques.

Forging of the alloy was conducted at 1000, 1050 and 1100 °C, corresponding to different volume fractions of the δ phase. At 1000 °C a peak stress at ~0.05 true strain was observed at all considered strain rates, followed by softening to a steady state flow condition at a true strain of ~0.5. Conversely, steady state flow behaviour was observed across all strain rates at 1050 and 1100 °C. Recrystallisation was not observed to have occurred and, therefore, dynamic recovery in the γ phase was believed to dominate steady state flow, with an activation energy of ~407 $kJmol^{-1}$. This value is significantly greater than the activation energy for self diffusion in nickel, but is thought to be a result of the high solute content (> 43 at% solute).

Flow softening has previously been related to microstructural evolution during TMP. However, no evidence of δ precipitate fragmentation was observed in the post-forged microstructures. Image analysis of the forged samples showed a significant reorientation of the δ precipitates, perpendicular to the forging axis, and this was thought to be the cause of the observed flow softening.

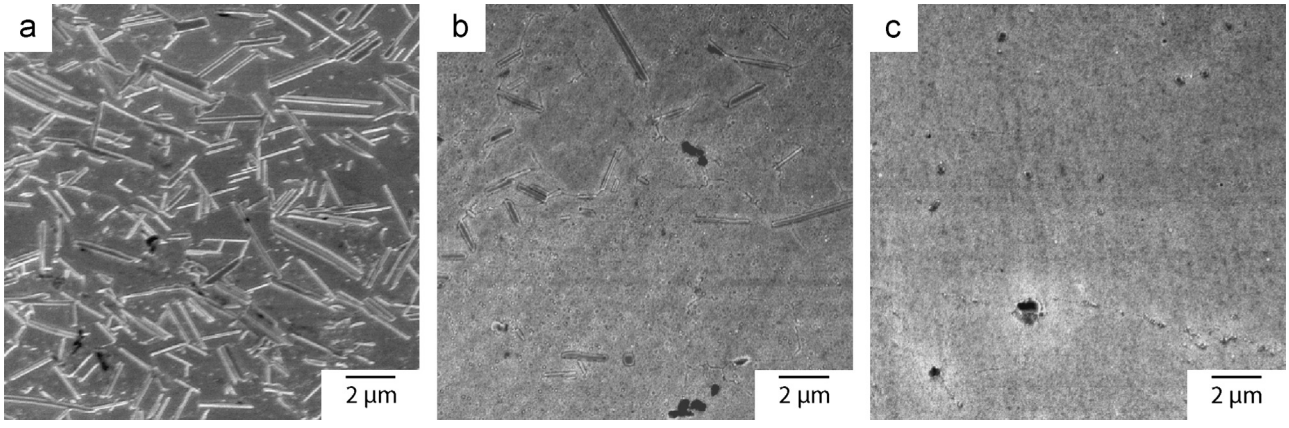

Fig. 8. SEI micrographs of V207M, imaged in the centre of the sample, following forging at a strain rate of 0.003 s^{-1} and a temperature of (a) 1000 °C, (b) 1050 °C and (c) 1100 °C, etched with phosphoric acid.

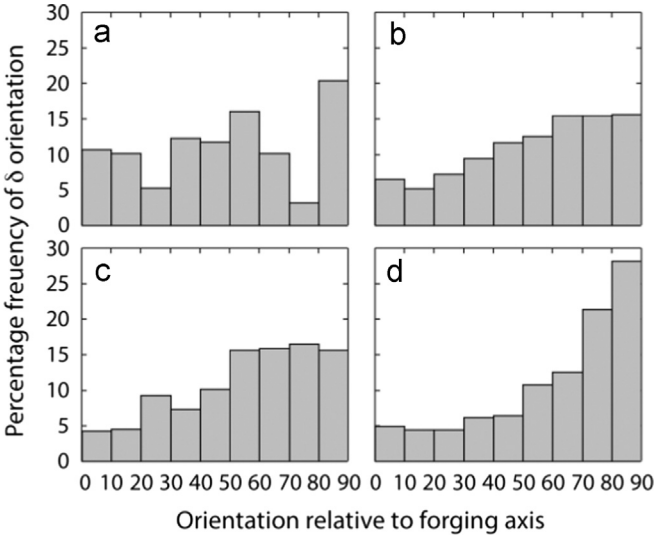

Fig. 9. Histograms showing the orientation distribution of the δ precipitates in (a) the as-HIP condition, and after forging at 1000 °C with strain rates of (b) 0.001 s^{-1}, (c) 0.003 s^{-1} and (d) 0.01 s^{-1}.

Acknowledgements

The authors would like to acknowledge M. Shakib for assistance with the forging and the EPSRC/Rolls-Royce Strategic Partnership for supporting this work through EP/H022309/1 and EP/H500375/1.

References

[1] European Aeronautics: A Vision for 2020, European Commission, 2001.
[2] Flightpath 2050 Europe's Vision for Aviation, European Commission, 2011.
[3] J.H. Perepezko, Science 326 (2009) 1068–1069.
[4] D.M. Dimiduk, D.B. Miracle, C.H. Ward, Mater. Sci. Technol. 8 (1992) 367–375.
[5] N.S. Stoloff, C.T. Liu, S.C. Deevi, Intermetallics 8 (2000) 1313–1320.
[6] D.M. Dimiduk, Mater. Sci. Eng. A 263 (1999) 281–288.
[7] J.Y. Hwang, R. Banerjee, J. Tiley, R. Srinivasan, G.B. Viswanathan, H.L. Fraser, Metall. Mater. Trans. A 40 (2009) 24–35.
[8] Y. Amouyal, Z. Mao, D.N. Seidman, Acta Mater. 58 (2010) 5898–5911.
[9] P.M. Mignanelli, N.G. Jones, M.C. Hardy, H.J. Stone, Mater. Sci. Eng. A 612 (2014) 179–186.
[10] H. Fecht, D. Furrer, Adv. Eng. Mater. 2 (12) (2000) 777–787.
[11] M.M. Allen, R.L. Atheby, J.B. Moore, Met. Eng. Q. 10 (1970) 20–30.
[12] D.R. Chang, D.D. Krueger, R.A. Sprague, Superalloys 1984 (1984) 245–273.
[13] J.M. Hyzak, R.P. Singh, J.E. Morra, T.E. Howson, Superalloys 1992 (1992) 93–101.
[14] J.W. Brooks, Mater. Des. 21 (2000) 297–303.
[15] C.A. Dandre, S.M. Roberts, R.W. Evans, R.C. Reed, Mater. Sci. Technol. 16 (2000) 14–16.
[16] S.L. Semiatin, K.E. McClary, A.D. Rollett, C.G. Roberts, E.J. Payton, F. Zhang, T.P. Gabb, Metall. Mater. Trans. A 44A (2013) 2778–2798.
[17] H. Yuan, W.C. Liu, Mater. Sci. Eng. A 408 (2005) 281–289.
[18] D. Huber, C. Stotter, C. Sommitsch, S. Mitsche, P. Poelt, B. Buchmayr, M. Stockinger, Superalloys 2008 (2008) 855–861.
[19] Y. Wang, W.Z. Shao, L. Zhen, B.Y. Zhang, Mater. Sci. Eng. A 528 (2011) 3218–3227.
[20] H.Y. Zhang, S.H. Zhang, M. Cheng, Z.X. Li, Mater. Charact. 61 (2010) 49–53.
[21] M. Detrois, R.C. Helmink, S. Tin, Mater. Sci. Eng. A 586 (2013) 236–244.
[22] H. Monajati, M. Jahazi, S. Yue, A.K. Taheri, Metall. Trans. A 36 (2005) 895–905.
[23] M.C. Hardy, European Patent Specification, EP2562277B1, 2014.
[24] D.L. Sponseller, Superalloys 1996 (1996) 259–270.
[25] R.M. Kearsey, A.K. Koul, J.C. Beddoes, C. Cooper, Superalloys 2000 (2000) 117–126.
[26] Y.V.R.K. Prasad, H.L. Gegel, S.M. Doraivelu, J.C. Malas, J.T. Morgan, K.A. Lark, D.R. Barker, Metall. Trans. A 14 (1984) 1883–1892.
[27] B. Marty, J.Y. Guedou, P. Gergaud, J.L. Lebrun, Superalloys 718, 625, 706 and Derivatives, 1997, pp. 331–342.
[28] C.I. Garcia, G.D. Wang, D.E. Camus, E.A. Loria, A.J. DeArdo, Superalloys 718, 625, 706 and Derivatives, 1994, pp. 293–302.
[29] C.M. Sellars, W.J. McTegart, Acta Metall. 14 (9) (1966) 1136–1138.
[30] M.J. Weis, M.C. Mataya, S.W. Thompson, D.K. Matlock, Superalloys 718 Metallurgy and Applications, 1989, pp. 135–154.
[31] Y. Ning, Z. Yao, X. Liang, Y. Liu, Mater. Sci. Eng. A 551 (2012) 1–12.
[32] A.J. Brand, K. Karhausen, R. Kopp, Mater. Sci. Technol. 12 (11) (1996) 963–969.
[33] C.M. Sellars, Philos. Trans. R. Soc. 288 (1978) 147–158.
[34] M.O. Alniak, F. Bedir, Mater. Des. 31 (2010) 1588–1592.
[35] J. Wang, J. Dong, M. Zhang, X. Xie, Mater. Sci. Eng. A 566 (2013) 61–70.
[36] S. Mitsche, C. Sommitsch, D. Huber, M. Stockinger, P. Poelt, Mater. Sci. Eng. A 528 (2011) 3754–3760.
[37] N.G. Jones, M. Jackson, Mater. Sci. Technol. 27 (6) (2011) 1025–1032.
[38] N.G. Jones, R.J. Dashwood, D. Dye, M. Jackson, Metall. Mater. Trans. A 40 (2009) 1944–1954.
[39] M. Jackson, N.G. Jones, D. Dye, R.J. Dashwood, Mater. Sci. Eng. A 501 (2009) 248–254.
[40] M. Sundararaman, P. Mukhopadhyay, S. Banerjee, Metall. Trans. A 19 (3) (1988) 453–465.